

ENHANCED DETECTABILITY OF PRE-REIONIZATION 21-CM STRUCTURE

MARCELO A. ALVAREZ¹, UE-LI PEN¹, AND TZU-CHING CHANG^{1,2}

Submitted to ApJ Letters June 30, 2010

ABSTRACT

Before the universe was reionized, it was likely that the spin temperature of intergalactic hydrogen was decoupled from the CMB by UV radiation from the first stars through the Wouthuysen-Field effect. If the IGM had not yet been heated above the CMB temperature by that time, then the gas would appear in absorption relative to the CMB. Large, rare sources of X-rays could inject sufficient heat into the neutral IGM, so that $\delta T_b > 0$ at comoving distances of tens to hundreds of Mpc, resulting in large 21-cm fluctuations with $\delta T_b \simeq 250$ mK on arcminute to degree angular scales, an order of magnitude larger in amplitude than that caused by ionized bubbles during reionization, $\delta T_b \simeq 25$ mK. This signal could therefore be easier to detect and probe higher redshifts than that due to patchy reionization. For the case in which the first objects to heat the IGM are QSOs hosting $10^7 - M_\odot$ black holes with an abundance exceeding $\sim 1 \text{ Gpc}^{-3}$ at $z \sim 15$, observations with either the Arecibo Observatory or the Five Hundred Meter Aperture Spherical Telescope (FAST) could detect and image their fluctuations at greater than $5\text{-}\sigma$ significance in about a month of dedicated survey time. Additionally, existing facilities such as MWA and LOFAR could detect the statistical fluctuations arising from a population of $10^5 - M_\odot$ black holes with an abundance of $\sim 10^4 \text{ Gpc}^{-3}$ at $z \simeq 10 - 12$.

Subject headings: cosmology: theory — dark ages, reionization, first stars — intergalactic medium

1. INTRODUCTION

The 21 cm transition is among the most promising probes of the high-redshift universe. The observed differential brightness temperature from the fully neutral IGM at the mean density with spin temperature $T_s(z)$ is given by

$$\delta T_b(z) \simeq 29 \text{ mK} \left(\frac{1+z}{10} \right)^{1/2} \left[1 - \frac{T_{\text{CMB}}(z)}{T_s(z)} \right] \quad (1)$$

(e.g., Madau et al. 1997). In the absence of an external radiation field, only the hot, dense gas in minihalos would have been able to develop a spin temperature different from that of the CMB at $z \sim 20$ (Shapiro et al. 2006). However, radiation emitted by the earliest generations of stars (e.g., Ciardi & Madau 2003; Barkana & Loeb 2005) and X-ray sources (Chuzhoy et al. 2006; Chen & Miralda-Escudé 2008) could have coupled the spin temperature to the IGM temperature via the “Wouthuysen-Field effect” (Wouthuysen 1952; Field 1959) long before reionizing the universe, at redshifts as high as $z = 20 - 30$, causing the IGM to appear in absorption with respect to the CMB, with $\delta T_b \simeq -250$ mK.

Only a modest amount of heating is necessary to raise the gas temperature above the CMB temperature of $\sim 30 - 60$ K at $z \sim 10 - 20$. By the time reionization was well underway, it is generally believed that the neutral component of the IGM had already been heated to $T_s \gg T_{\text{CMB}}$, and therefore the observed brightness temperature will be an order of magnitude lower in amplitude, $\delta T_b \simeq 25$ mK, than when the IGM was in absorption (e.g., Furlanetto et al. 2006).

Clearly, there should be some transition epoch, during which sources of X-ray radiation heated the neutral IGM, creating “holes” in the absorption. Natural candidates for these early sources of heating are quasars (e.g., Chuzhoy et al. 2006; Zaroubi et al. 2007; Thomas & Zaroubi 2008; Chen & Miralda-Escudé 2008). Unfortunately, little is known about

the quasar population at $z > 6$, with the only constraints coming from the bright end at $z \sim 6$ (e.g., Fan et al. 2002; Willott et al. 2010), with inferred black hole masses $\gtrsim 10^8 M_\odot$, luminosities $\gtrsim 10^{46} \text{ erg s}^{-1}$, and a comoving abundance $\gtrsim 1 \text{ Gpc}^{-3}$.

Quasars are not the only high-redshift objects able to produce X-rays. High-redshift supernovae (Oh 2001) and X-ray binaries could have also been sources. Theoretical models typically parametrize X-ray production associated with star formation by f_X , normalized so that $f_X = 1$ corresponds to that observed for local starburst galaxies (e.g., Furlanetto 2006; Pritchard & Furlanetto 2007).

Our aim in this paper is to explore the enhanced 21-cm signature of early quasars. We will therefore assume that the first galaxies were efficient enough to couple the spin temperature to the kinetic temperature by $z \simeq 20$, but did not heat the IGM above the CMB temperature, i.e. $f_X \ll 1$. As shown by Pritchard & Loeb (2010), even for values of $f_X > 1$ it is still possible that there is a significant period between the time when the spin temperature was coupled to the kinetic temperature and the time when the mean IGM was heated above the CMB temperature. In addition, the first galaxies were likely clustered around the quasars and may have actually increased the sizes of the heated regions. On the other hand, X-ray-emitting galaxies could have also formed outside the regions that would have been heated by the quasars, making the 21-cm features due to early, rare quasars that we predict here less prominent.

This paper is organized as follows. In §2 we present our forecasted signal from partially-heated regions and a brief discussion of the expected black hole abundance at high-redshift. In §3 we assess the detectability of the predicted signal under various assumptions about the early quasar population. We end in §4 with a discussion of possible survey strategies and requirements of detection on the high-redshift black hole abundance. All calculations were done assuming a flat universe with $(\Omega_m h^2, \Omega_b h^2, h, n_s, \sigma_8) = (0.133, 0.0225, 0.71, 0.96, 0.8)$, consistent with WMAP 7-year data (Komatsu et al. 2010). All distances are comoving.

Electronic address: malvarez@cita.utoronto.ca

¹ Canadian Institute for Theoretical Astrophysics, University of Toronto, 60 St. George St., Toronto, ON M5S 3H8, Canada

² IAA, Academia Sinica, PO Box 23-141, Taipei, 10617, Taiwan

2. FORECAST

Our predictions will focus on accreting black holes with masses greater than $\simeq 10^5 M_\odot$. It is of course possible that a more abundant population of black holes with lower masses existed at these early times, left behind as remnants of early generations of massive Pop III stars (Heger et al. 2003), acting as “seeds” for the observed $z \sim 6$ supermassive black hole population (e.g., Li et al. 2007), and powering “miniquasars” (Madau et al. 2004). However, radiative feedback from the progenitor stars (Johnson & Bromm 2007) as well as the accretion radiation itself (Alvarez et al. 2009), would have likely substantially limited their growth and corresponding X-ray emission at early times. An alternative scenario for forming the seeds is gaseous collapse to black holes with masses greater than $\simeq 10^4 M_\odot$ in the first halos with virial temperature greater than $\simeq 10^4$ K (e.g., Bromm & Loeb 2003; Begelman et al. 2006). Formation of black holes by this mechanism may have been quite a rare occurrence (e.g., Dijkstra et al. 2008). It is this scenario, in which most accreting black holes in the universe were relatively rare and more massive than $\simeq 10^5 M_\odot$, that is most consistent with the predictions we make here.

Because the heating is a time-dependent effect, we will parametrize the total energy radiated during accretion as $E_{\text{tot}} = Lt_{\text{QSO}} = \epsilon M_{\text{BH}} c^2$, where we take the radiative efficiency $\epsilon = 0.1$. In principle some of the rest mass energy, i.e. the initial seed mass of the black hole, did not contribute to heating the surroundings, but in general the seed mass is expected to be small compared to the mass of the black hole after it undergoes its first episode of radiatively-efficient accretion as a quasar, so we neglect it.

2.1. Quasar spectral energy distribution

We assume the spectral energy distribution of the quasar is given by a broken power-law, $S_\nu \propto \nu^{-0.5}$ at $\nu < \nu_b$, and $S_\nu \propto \nu^{-1.5}$ at $\nu > \nu_b$, with $h\nu_b = 11.8$ eV (e.g., Bolton & Haehnelt 2007), approximately consistent with the template spectra of Telfer et al. (2002). If the quasar has a total bolometric luminosity L , then the spectral energy distribution is

$$S_\nu = \frac{L}{4\nu_b} \begin{cases} (\nu/\nu_b)^{-0.5}, & \nu < \nu_b, \\ (\nu/\nu_b)^{-1.5}, & \nu > \nu_b. \end{cases} \quad (2)$$

2.2. The 21-cm profile around individual quasars

The temperature profile surrounding a quasar can be obtained by considering the fraction of the radiated energy absorbed per atom at comoving distance r and redshift z ,

$$\Gamma_{\text{HI}}(r, z) = \frac{(1+z)^2}{4\pi L r^2} \int_{\nu_{\text{HI}}}^{\infty} d\nu \frac{S_\nu \sigma_\nu}{h\nu} (h\nu - h\nu_{\text{HI}}) \chi_\nu \exp[-\tau_\nu(r)], \quad (3)$$

where χ_ν is the fraction of photoelectron energy, $h\nu - h\nu_{\text{HI}}$, which goes into heat, with the rest being lost to secondary ionizations and excitations. In the limit in which the ionized fraction of the gas is low, $0.1 < \chi_\nu < 0.3$ for all $h\nu > 25$ eV (Shull & van Steenberg 1985). In what follows we will make the approximation that $S_\nu = 0.2$ for all ν , and assume that the energy radiated is $Lt_{\text{qso}} \equiv \epsilon M_{\text{BH}} c^2$, with t_{qso} short compared to the Hubble time. In this case, the relative brightness temperature is given by

$$\delta T_b(M_{\text{BH}}, r, z) = 29 \text{ mK} \left[1 - \frac{T_{\text{CMB}}(z)}{T_s(M_{\text{BH}}, r, z)} \right] \left[\frac{1+z}{10} \right]^{1/2}, \quad (4)$$

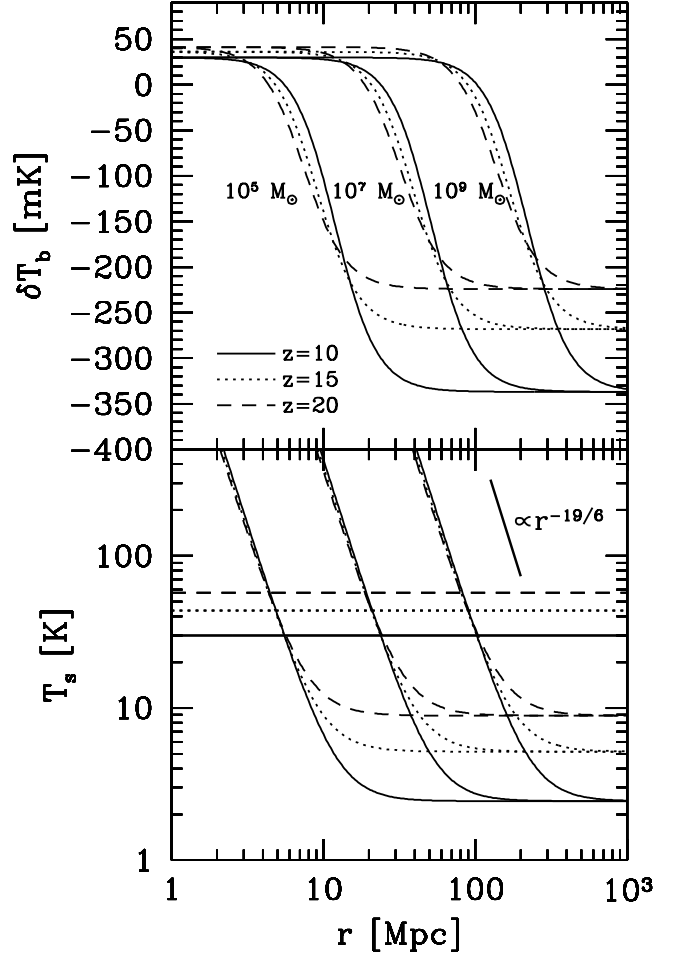


FIG. 1.— Top: Profiles of the observed differential brightness temperature versus comoving distance at three different redshifts around a quasar that has radiated 10 per cent of the rest-mass energy of 10^5 , 10^7 , and $10^9 M_\odot$, as labeled. Bottom: Spin temperature of the IGM, obtained via equation (5).

where

$$T_s(M_{\text{BH}}, r, z) = T_{\text{IGM}}(z) + \frac{2\epsilon M_{\text{BH}} c^2}{3k_b} \Gamma_{\text{HI}}(r, z). \quad (5)$$

In calculating the optical depth, we assume that the IGM is completely neutral at the mean density, $n_{\text{H}}(z)$, so that $\tau_\nu(r, z) = n_{\text{H}}(z)(1+z)^{-1} \sigma_\nu$. In reality, the quasar’s own H II region will reduce the opacity at small radii, but given that we are concerned with the small amount of heating happening at much larger radii, we neglect the H II region when calculating the optical depth.

Shown in Fig. 1 are profiles of the observed differential brightness temperature versus comoving distance at three different redshifts. The total energy radiated by the quasar, Lt_{QSO} in each curve corresponds to 10 per cent of the rest mass, as labeled. Close to the quasar, the gas is heated above the CMB temperature, and $\delta T_b \simeq 30$ – 40 mK. Further away, the heating from the quasar declines due to spherical dilution and attenuation of the lowest energy radiation, with δT_b finally reaching about -220 to -340 mK at large distances. The FWHM size of the fluctuations are about 20, 80, and 400 Mpc for black holes of mass 10^5 , 10^7 , and $10^9 M_\odot$, respectively.

2.3. Black hole abundance at high- z

How do the black hole densities and masses we assume here compare to those observed at $z \sim 6$ and expected at higher redshifts? Willott et al. (2010) constructed the mass function of black holes in the range $10^8 M_\odot < M_{\text{BH}} < 3 \times 10^9 M_\odot$ at $z = 6$, finding it to be well-fitted by $dn/d\ln M_{\text{BH}} \simeq \phi_* (M_{\text{BH}}/M_*)^{-1} \exp(-M_{\text{BH}}/M_*)$, with $\phi_* = 5.34 \text{ Gpc}^{-3}$ and $M_* = 2.2 \times 10^9 M_\odot$. Integrating the black hole mass function, one finds $\rho_{\text{BH}}(> M_{\text{BH}}) \simeq 7 \times 10^9$ and $3 \times 10^{10} M_\odot \text{ Gpc}^{-3}$, for $M_{\text{BH}} = 10^9$, and $10^8 M_\odot$, respectively, somewhat larger than the black hole mass density we find which maximizes the 21-cm power spectrum (§3.2). Matching the abundance of black holes greater than a given mass to the dark matter halo mass function of Warren et al. (2006) at $z = 6$ (“abundance matching” – e.g., Kravtsov et al. 2004), we obtain $M_{\text{halo}} = 2.3 \times 10^{12}$ and $4.7 \times 10^{12} M_\odot$ for $M_{\text{BH}} = 10^8$ and $10^9 M_\odot$, respectively, implying a value of $M_{\text{BH}}/M_{\text{halo}} \simeq 4 \times 10^{-5}$ to 2×10^{-4} over the same range.

More detailed predictions would require extrapolating the $M_{\text{BH}} - M_{\text{halo}}$ relationship to lower masses and higher redshifts, or making highly uncertain assumptions about the formation mechanism of the high-redshift seeds and their accretion history. For example, the ratio $M_{\text{BH}}/M_{\text{halo}} \simeq 10^{-4}$ we determine here by abundance matching at $z = 6$ and $M_{\text{BH}} = 10^8 - 10^9 M_\odot$ would be a significant underestimate in atomic cooling halos where black hole formation by direct collapse took place, in which it is possible that $M_{\text{BH}}/M_{\text{halo}}$ could approach the limiting value of $\Omega_b/\Omega_m \simeq 0.17$. Clearly much more work is required in understanding the high-redshift quasar population, and for this reason the constraints provided by either detection or non-detection of the signal we predict here would be very valuable.

3. DETECTABILITY

In this section, we estimate the detectability of individual sources as well the statistical detection of their power spectrum. In the case of individual objects, we focus on a novel approach, using single-dish filled aperture telescopes like Arecibo³ and FAST⁴, while for the power spectrum we will simply refer to existing sensitivity estimates for facilities such as LOFAR⁵, MWA⁶, and SKA⁷.

3.1. Individual quasars

In order to determine the necessary integration time, we convolve the profiles shown in Fig. 1 with a half-power beam width of

$$\theta_b = 26' \left(\frac{1+z}{11} \right) \left(\frac{d_{\text{dish}}}{300 \text{ m}} \right)^{-1}, \quad (6)$$

where d_{dish} is the effective dish diameter. Converting angle on the sky to comoving distance, we obtain the comoving resolution,

$$D \simeq 70 \text{ Mpc} \left(\frac{d_{\text{dish}}}{300 \text{ m}} \right)^{-1} \left(\frac{1+z}{11} \right)^{1.2}. \quad (7)$$

This implies that the fluctuation created by a $10^7 M_\odot$ -black hole would be just resolvable with a single 300-m dish like

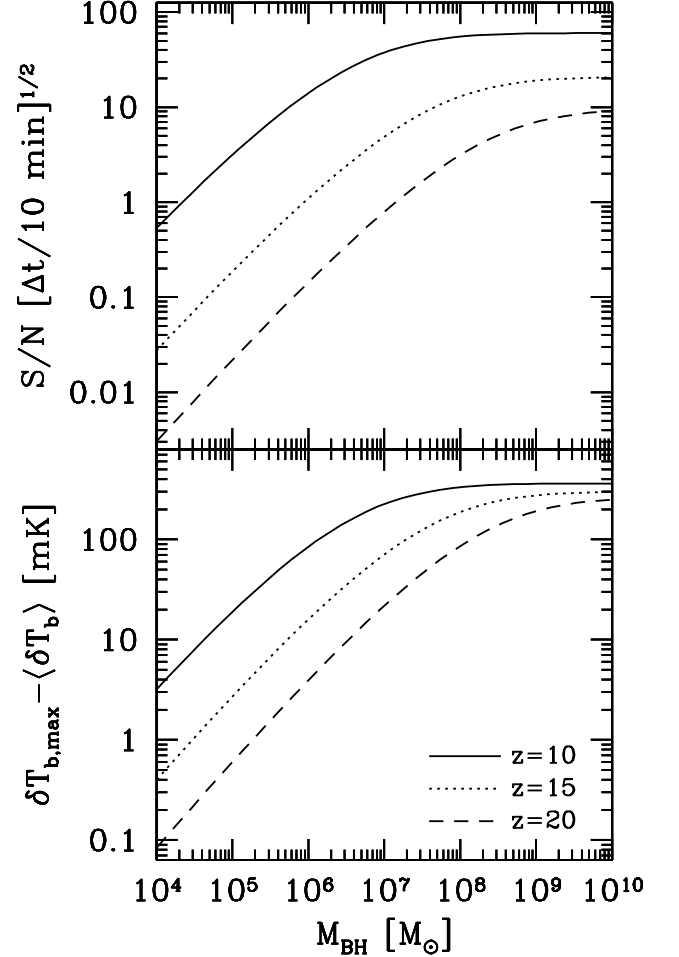


FIG. 2.— Bottom: Peak fluctuation amplitude, measured with respect to the mean background absorption $\langle \delta T_b \rangle(z)$, as a function of black hole mass, for three different redshift. Top: Signal-to-noise ratio at the same redshifts for a bandwidth corresponding to the beam width and an integration time of 10 minutes. The detectability declines rapidly in the interval $10 < z < 20$.

Arecibo (see Fig. 1), lower mass black holes would be unresolved point sources, and the profile of higher mass black holes could actually be measured. For an integration time of Δt , the sensitivity is given by

$$\delta T_{\text{err}} = 22 \text{ mK} \left(\frac{\Delta t}{60 \text{ s}} \right)^{-1/2} \left(\frac{d_{\text{dish}}}{300 \text{ m}} \right)^{1/2} \left(\frac{1+z}{11} \right)^{2.35} \quad (8)$$

where we have used

$$\Delta \nu = 4 \text{ MHz} \left(\frac{D}{70 \text{ Mpc}} \right) \left(\frac{1+z}{11} \right)^{-1/2} \quad (9)$$

for the bandwidth corresponding to a comoving distance D , $\delta T_{\text{err}} = T_{\text{sys}}/\sqrt{\Delta \nu \Delta t}$, and $T_{\text{sys}} \simeq 3 \times 10^5 \text{ mK} [(1+z)/11]^{2.7}$ (e.g., Furlanetto et al. 2006).

We calculate the maximum fluctuation amplitude as a function of quasar black hole mass and redshift, $\delta T_{\text{b,max}}(M_{\text{bh}}, z)$, which is a convolution of the beam with the individual profiles plotted in Fig. 1,

$$\delta T_{\text{b,max}} = \frac{2}{\theta_b^2 D} \int_0^\infty d\theta \theta e^{-\frac{\theta^2}{2\theta_b^2}} \int_0^{D/2} dl \delta T_b(r_{l\theta}), \quad (10)$$

where we use a Gaussian profile with a FWHM of $\theta_b(z)$, such

³ <http://www.naic.edu>

⁴ <http://fast.bao.ac.cn>

⁵ <http://www.lofar.org>

⁶ <http://www.mwatelescope.org>

⁷ <http://www.skatelescope.org>

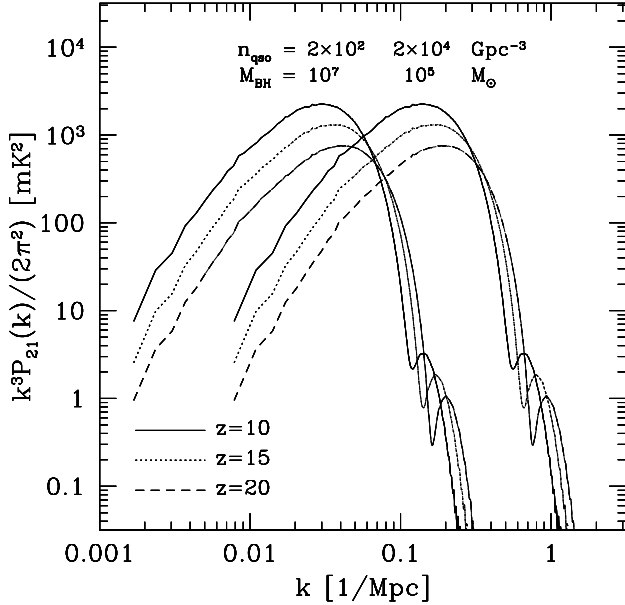


FIG. 3. — Shown is the spherically-averaged three-dimensional power spectrum of 21-cm fluctuations for a black hole density $1 M_{\odot}/\text{Mpc}^3$, for three different redshifts, as labeled. Large, relatively rare $10^7 M_{\odot}$ black holes have a power spectrum which peaks at $k \sim 0.03 \text{ Mpc}^{-1}$, while for $M_{\text{BH}} = 10^5 M_{\odot}$ the power spectrum which peaks at $k \sim 0.15 \text{ Mpc}^{-1}$. Such a signal at $z = 10$ should be easily detectable by LOFAR, MWA, or SKA.

that $\theta_b(z) = 2\sqrt{2\ln 2}\theta_g(z)$, and $r_{l\theta}^2 = r_{\theta}^2 + l^2$, where r_{θ} is the projected comoving distance perpendicular to the line of sight corresponding to the angle θ .

Shown in Fig. 2 are the resulting fluctuation amplitudes with respect to the mean background absorption, $\delta T_{\text{b,max}}(M_{\text{bh}}, z) - \langle \delta T_b \rangle(z)$, as well as the signal-to-noise ratio, $[\delta T_{\text{b,max}}(M_{\text{bh}}, z) - \langle \delta T_b \rangle(z)] / \delta T_{\text{b,err}}(z)$ for an integration time of 10 minutes. As can be seen from the figure both the signal, and to a greater extent the signal-to-noise, decline rapidly with increasing redshift. This is due to several reasons. First, the intrinsic signal declines with increasing redshift because absorption is relatively weaker at higher redshifts when the IGM has not had as much time to cool (see Fig. 1). In addition, the beamwidth gets larger, in proportion to $1+z$, while the angular size of the fluctuations at fixed black hole mass actually decline with redshift, as seen from Fig. 1.

3.2. Power spectrum from Poisson fluctuations

To estimate the fluctuating background from a superposition of sources, we assume all black holes at a given redshift have the same mass, M_{BH} , and comoving number density, n_{BH} . We then generate a realization of random black hole positions within a periodic box, and calculate the heating from each source using equation (5). Because the heating rate is proportional to mass and we assume a random spatial distribution, the two length scales in the system are the mean separation of sources, $r_{\text{sep}} \propto n_{\text{BH}}^{-1/3}$, and the distance to which an individual black hole can effectively heat the IGM above the CMB temperature, $r_{\text{heat}} \propto M_{\text{BH}}^{1/3}$. For this simplified case, in which the spatial distribution of black holes is random and all black holes have the same mass, the shape of the power spectrum is determined only by the ratio $r_{\text{heat}}/r_{\text{sep}} \propto (n_{\text{BH}} M_{\text{BH}})^{1/3} = \rho_{\text{BH}}^{1/3}$. Our choice of $\rho_{\text{BH}} = 2 \times 10^9 M_{\odot} \text{Gpc}^{-3}$ is

roughly that density at which the signal is maximized; a lower black hole mass density results in a lower overall signal, while a higher density leads to overlap of the individual regions, and the fluctuations become saturated.

Shown in Fig. 3 is our predicted power spectrum for Poisson fluctuations of black holes of mass $M_{\text{BH}} = 10^5$ and $10^7 M_{\odot}$ at $z = 10, 15$, and 20 . Because the black hole mass density is the same in both cases, the curves have the same shape, but are shifted in wavenumber such that $k^{-3} \propto M_{\text{BH}}$. Because the individual regions are only weakly overlapping for $\rho_{\text{BH}} = 2 \times 10^9 M_{\odot} \text{Gpc}^{-3}$, the shape of the curve is quite close to the Fourier transform of an individual region, so that

$$P(k)^{1/2} \propto \int_0^{\infty} r^2 dr \delta T_b(r) \frac{\sin kr}{kr}, \quad (11)$$

with $\delta T_b(r)$ given by eqs. (4) and (5).

The amplitude of this signal at $k \sim 0.1 \text{ Mpc}^{-1}$ ($[k^3 P(k)/(2\pi^2)]^{1/2} \simeq 50 \text{ mK}$) is almost an order of magnitude greater than that expected from ionized bubbles when $T_S \gg T_{\text{CMB}} (\simeq 6 \text{ mK})$, e.g., Furlanetto et al. 2004), which compensates for the increased foregrounds at the higher redshifts corresponding to the signal we predict here. For example, McQuinn et al. (2006) estimated the sensitivity of various facilities to the spherically-averaged power spectrum, finding (at $z = 12$) $\delta T_{\text{b,err}}^2(k \sim 0.1 \text{ Mpc}^{-1}) \simeq 30 \text{ mK}^2$ for LOFAR and MWA, and $T_{\text{b,err}}^2(k \sim 0.1 \text{ Mpc}^{-1}) \simeq 0.1 \text{ mK}^2$ for SKA, for their adopted array configurations and 1000 hr of integration time (Fig. 6 and Table 1 of McQuinn et al. 2006). Thus, the power spectrum shown in Fig. 4 would be easily detectable by either of these three experiments at $z \sim 12$ for the survey parameters used by McQuinn et al. (2006).

4. SURVEY STRATEGIES

Since the signal comes from a large angular scale on the sky, a filled aperture maximizes the sensitivity. The two largest collecting area telescopes are Arecibo and, under construction, FAST. They are at latitudes $\delta = 18$ (26) degrees, respectively. To stabilize the baselines, a drift scan at 80 MHz maps a strip of width 40 (90) arc minutes by length 360 degrees $\cos \delta$ every day. With Arecibo, a custom feedline with pairwise correlations of dipoles would allow a frequency independent illumination of the mirror, allowing the frequency independent removal of foregrounds. It would also allow operation as an interferometer, increasing stability and rejection of interference, and enabling arbitrary apodization of the surface. Should grating sidelobes from support structures become a problem, one could also remove the carriage house, and mount the feedline on a pole from the center of the dish. This would result in a clean, unblocked aperture with frequency independent beam. Even with the carriage support blocking, the side lobes would still be frequency independent for an appropriately scaled illumination pattern.

For FAST, a focal plane array also enables a frequency independent illumination of the primary, resulting in a frequency independent beam on the sky. It also increases the survey speed by the number of receivers used. Only one receiver is needed every half wave length, roughly two meters. Hundred pixel surveys seem conceivable at low cost, since only small bandwidths would be needed, and the system temperature is sky limited, even with cheap TV amplifiers.

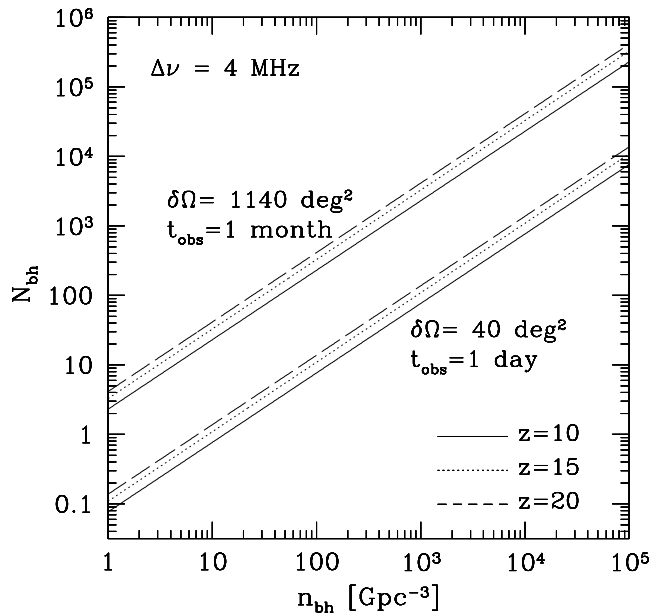


FIG. 4.— Number of black holes expected within a 1-month (upper curves) and 1-day (lower curves) survey in drift-scan mode that scans each point in the sky nine times, as a function of comoving black hole density. The integration time per pixel in each case is about 7, 14, and 25 minutes for $z = 10, 15,$ and 20 . With a 14-minute integration time, a $10^7 - M_{\odot}$ black hole would be detectable at greater than $5\text{-}\sigma$ significance (see Fig. 2)

We note that the ratio of signal to foreground in this regime is comparable to that during reionization. With a filled aperture, it may be easier to achieve foreground subtraction. This has been demonstrated for intensity mapping at $z \sim 0.8$ using the filled aperture of GBT (Chang et al. 2010), where a similar foreground ratio exists of galactic synchrotron to 21cm.

Shown in Fig. 4 is the expected number of black holes within the field of view for a given redshift and survey bandwidth, versus their comoving number density. A dedicated

one month survey operating at 88 MHz ($z \sim 15$) with a 300-m dish like Arecibo, which scans each point in the sky nine times would have a pixel size of about 0.4 deg^2 during which each pixel was integrated for about 15 minutes and 1140 deg^2 were surveyed. If $10^7 - M_{\odot}$ black holes had a number density of 1 Gpc^{-3} at that time, one would expect to discover about three or four of them at greater than $5\text{-}\sigma$ significance since each pixel would have been integrated for about 15 minutes at $z = 15$ (see dotted lines in Figs. 2 and 4). Black holes with masses greater than $10^7 M_{\odot}$ and similar abundances would be easily detectable, allowing for followup with longer baseline facilities such as LOFAR to determine the detailed shape of their 21-cm profile. Detecting a $10^6 - M_{\odot}$ black hole at $5\text{-}\sigma$ significance would require a significantly longer integration time on each pixel, about 4 hours, so that only about 70 deg^2 could be surveyed in a month. Thus, the minimum spatial density of $10^6 - M_{\odot}$ black holes would be about 5 Gpc^{-3} at $z = 15$. Smaller black holes would mean even smaller fields of view and longer integration times per pixel, so in those cases detecting their statistical signature in the spherically-averaged power spectrum discussed in §3.2 may be a better approach.

Regardless of whether high-redshift quasar X-ray sources will be detected directly by the means we propose here, it is clear that the pre-reionization universe offers a wealth of information that can be uniquely probed with the 21-cm transition, and it is therefore vital that theoretical models for the signal originating from before the epoch of reionization continue to be developed.

We wish to thank J. Peterson and R. M. Thomas for helpful discussions on Arecibo and 21-cm signatures of early QSOs, respectively, and J. R. Pritchard for comments on an earlier draft of the paper. M. A. A. and T. C. are grateful for the hospitality of the Aspen Center for Physics, where this work was completed. We acknowledge financial support by CfAR and NSERC.

REFERENCES

- Alvarez, M. A., Wise, J. H., & Abel, T. 2009, *ApJ*, 701, L133
 Barkana, R. & Loeb, A. 2005, *ApJ*, 626, 1
 Begelman, M. C., Volonteri, M., & Rees, M. J. 2006, *MNRAS*, 370, 289
 Bolton, J. S. & Haehnelt, M. G. 2007, *MNRAS*, 374, 493
 Bromm, V. & Loeb, A. 2003, *ApJ*, 596, 34
 Chang, T.-C., Pen, U.-L., Bandurak, K., & Peterson, J. 2010, *Nature*, in press
 Chen, X. & Miralda-Escudé, J. 2008, *ApJ*, 684, 18
 Chuzhoy, L., Alvarez, M. A., & Shapiro, P. R. 2006, *ApJ*, 648, L1
 Ciardi, B. & Madau, P. 2003, *ApJ*, 596, 1
 Dijkstra, M., Haiman, Z., Mesinger, A., & Wyithe, J. S. B. 2008, *MNRAS*, 391, 1961
 Fan, X., Narayanan, V. K., Strauss, M. A., White, R. L., Becker, R. H., Pentericci, L., & Rix, H.-W. 2002, *AJ*, 123, 1247
 Field, G. B. 1959, *ApJ*, 129, 536
 Furlanetto, S. R. 2006, *MNRAS*, 371, 867
 Furlanetto, S. R., Oh, S. P., & Briggs, F. H. 2006, *Phys. Rep.*, 433, 181
 Furlanetto, S. R., Zaldarriaga, M., & Hernquist, L. 2004, *ApJ*, 613, 1
 Heger, A., Fryer, C. L., Woosley, S. E., Langer, N., & Hartmann, D. H. 2003, *ApJ*, 591, 288
 Johnson, J. L. & Bromm, V. 2007, *MNRAS*, 374, 1557
 Komatsu, E. et al. 2010, *ApJ*, submitted, arXiv:1001.4538
 Kravtsov, A. V., Berlind, A. A., Wechsler, R. H., Klypin, A. A., Gottlöber, S., Allgood, B., & Primack, J. R. 2004, *ApJ*, 609, 35
 Li, Y., Hernquist, L., Robertson, B., Cox, T. J., Hopkins, P. F., Springel, V., Gao, L., Di Matteo, T., Zentner, A. R., Jenkins, A., & Yoshida, N. 2007, *ApJ*, 665, 187
 Madau, P., Meiksin, A., & Rees, M. J. 1997, *ApJ*, 475, 429
 Madau, P., Rees, M. J., Volonteri, M., Haardt, F., & Oh, S. P. 2004, *ApJ*, 604, 484
 McQuinn, M., Zahn, O., Zaldarriaga, M., Hernquist, L., & Furlanetto, S. R. 2006, *ApJ*, 653, 815
 Oh, S. P. 2001, *ApJ*, 553, 499
 Pritchard, J. R. & Furlanetto, S. R. 2007, *MNRAS*, 376, 1680
 Pritchard, J. R. & Loeb, A. 2010, *ArXiv e-prints*
 Shapiro, P. R., Ahn, K., Alvarez, M. A., Iliev, I. T., Martel, H., & Ryu, D. 2006, *ApJ*, 646, 681
 Shull, J. M. & van Steenberg, M. E. 1985, *ApJ*, 298, 268
 Telfer, R. C., Zheng, W., Kriss, G. A., & Davidsen, A. F. 2002, *ApJ*, 565, 773
 Thomas, R. M. & Zaroubi, S. 2008, *MNRAS*, 384, 1080
 Warren, M. S., Abazajian, K., Holz, D. E., & Teodoro, L. 2006, *ApJ*, 646, 881
 Willott, C. J., Albert, L., Arzoumanian, D., Bergeron, J., Crampton, D., Delorme, P., Hutchings, J. B., Omont, A., Reyle, C., & Schade, D. 2010, *ArXiv e-prints*
 Wouthuysen, S. A. 1952, *AJ*, 57, 31
 Zaroubi, S., Thomas, R. M., Sugiyama, N., & Silk, J. 2007, *MNRAS*, 375, 1269